Microchemical Journal 204 (2024) 111106

Contents lists available at ScienceDirect

Microchemical Journal

journal homepage: www.elsevier.com/locate/microc

Simultaneous electrochemical detection of hydroquinone and catechol using flexible laser-induced metal-polymer composite electrodes

Maria Kaneva [a], Aleksandra Levshakova [a], Ilya Tumkin [a,b], Maxim Fatkullin [c], Evgeny Gurevich [d,e], Alina Manshina [a], Raul D. Rodriguez [c], Evgeniia Khairullina [a,f,*]

[a] Institute of Chemistry, Saint Petersburg State University, Universitetskaya nab. 7/9, St. Petersburg 199034, Russia
[b] Applied Laser Technologies, Ruhr University Bochum, Universitätsstr. 150, Bochum 44801, Germany
[c] Tomsk Polytechnic University, Lenin Ave. 30, Tomsk 634050, Russia
[d] Laser Center (LFM), University of Applied Sciences Münster, Stegerwaldstraße 39, 48565 Steinfurt, Germany
[e] Center for Laser and Optics, Anhui University, Hefei 230088, China
[f] School of Physics and Engineering, ITMO University, Lomonosova 9, Saint-Petersburg 191002, Russia

ARTICLE INFO

Keywords:
Flexible sensor
Laser-induced graphene
Laser fabrication
Hydroquinone
Catechol
Water pollution

ABSTRACT

The conversion of waste polymers into functional materials presents a promising approach for PET upcycling. In this study, we exploit PET transformed into a Laser-Induced Graphene/Al NPs/PET nanocomposite (LIMPc – Laser-Induced Metal-Polymer composite) modified with electrodeposited gold nanoparticles (AuNPs). The morphology and structure of the material were investigated by scanning electron microscopy (SEM), energy-dispersive X-ray (EDX), and X-ray photoelectron spectroscopy (XPS). The nanocomposite was employed as a flexible electrochemical sensor for the simultaneous electrochemical detection of hydroquinone (HQ) and catechol (CT). The LIMPc-plasma-NaOH-Au composite displayed well-defined oxidation peaks for HQ and CT during electrochemical analysis, with limits of detection (LOD) as low as 47 nM for CT and 56 nM for HQ, within a linear range of 0.1–300 μM for both compounds. The long-term stability of LIMPc-plasma-NaOH-Au and its performance in real sample analysis demonstrate its potential for environmental monitoring applications.

1. Introduction

Catechol (CT) and hydroquinone (HQ) are widely used in producing various goods, including leather, pharmaceuticals, dyes, and cosmetics. [1]. These isomers are known for their high toxicity, resistance to degradation, and long-term adverse effects on human health. Over-exposure to HQ and CT can result in fatigue, tachycardia, liver damage, kidney dysfunction, and other health issues [2,3]. During production and usage, these compounds may be released into groundwater and rivers, causing environmental pollution. According to the European Chemical Agency (ECHA), hydroquinone (HQ) is classified under several categories of hazardous substances, such as health hazard (GHS07), serious hazard for human health (GHS08), corrosive (GHS05), and hazardous to the environment (GHS09) [4]. Hydroquinone exhibits high levels of ecotoxicity (for instance, less than 1 mg/liter for several aquatic species), and this toxicity significantly fluctuates across different species [5]. Catechol can also inhibit the growth of microorganisms and be lethal to aquatic organisms at relatively low concentrations, starting from the micromolar range per liter [6,7]. Therefore, there is a need for the efficient quantitative determination of HQ and CT in real life samples [8].

Various analytical techniques have been tested to address this need, including fluorescence, high-performance liquid chromatography, and spectrophotometry [2,9]. However, these methods have limitations, including expensive equipment, time-consuming sample preparation, and analytical protocols. In contrast, electrochemical detection offers several advantages, such as rapid response, low cost, high sensitivity and selectivity [10–14].

Glassy-carbon electrodes (GCEs) are widely used in conventional electrochemical sensors and often deliver excellent performance under optimal conditions with appropriate modifications [10,15,16]. However, the fabrication and pretreatment of these electrodes can be labor-intensive and complex. As a result, there has been a growing interest in flexible systems, such as portable sensors for on-site analysis and online monitoring [17–20]. Flexible electrochemical sensors integrated with nanomaterials have demonstrated great promise in various

* Corresponding author at: Institute of Chemistry, Saint Petersburg State University, 5 Ulyanovskaya St., St. Petersburg 198504, Russia.
E-mail address: e.khayrullina@spbu.ru (E. Khairullina).

https://doi.org/10.1016/j.microc.2024.111106
Received 17 January 2024; Received in revised form 26 June 2024; Accepted 29 June 2024
Available online 30 June 2024

applications, including implantable and wearable devices for real-time, non-invasive detection of analytes in biological samples [21–30]. Among various flexible polymers, polyethylene terephthalate (PET), is widely used as a substrate for electrode fabrication due to its affordability, simple production process, transparency, and mechanical stability [12,13,31–35].

Not surprisingly, the aforementioned properties open the way for PET applications not only in sensors but also in many other fields. However, the disposal of PET in the environment presents serious challenges, as it can take hundreds of years to decompose naturally. Improper management of PET waste can lead to significant damage to marine ecosystems through the formation of microplastics. It is crucial to find sustainable solutions for the post-utilization of PET to mitigate its environmental impact and reduce the need for landfilling or incineration [36–39]. Developing innovative methods to upcycle PET waste into valuable materials can contribute to addressing these environmental concerns while also expanding the range of PET applications.

A promising approach for PET upcycling is the transformation of waste polymers into new functional materials. Recent research has focused on finding alternatives to traditional methods of incorporating plastic residues into building products [40]. These alternatives include [41] (i) the production of value-added chemicals, (ii) the development of composite materials with improved properties for high-end applications, and (iii) the conversion of waste polymers into carbon-based advanced materials [42,43].

Among the various conversion approaches, laser-assisted synthesis has emerged as a promising method [44–50] for fabricating advanced carbon-based nanomaterials such as graphene [44], carbon nanotubes (CNTs), and laser-induced metal-polymer composites (LIMPc) [51–55]. The latter material exhibits exceptional functional properties, including high conductivity and mechanical strength, making it highly suitable for application in electrochemical sensors. Furthermore, the laser-based fabrication process enables the transformation of the outer polymer layer while preserving the integrity of the bulk polymer substrates, resulting in excellent adhesion properties of the electrocatalytically active layer.

To our knowledge, there are limited reports on flexible sensors for catechol (CT) and hydroquinone (HQ) detection [56,57]. Flexible systems can be used in wearable electronics, for example by workers in factories, or applied to plants to monitor the composition of groundwater [22]. Flexible electrodes can also be applied to non-planar surfaces, such as the inside of aquifer channels or pipelines for detecting wastewater pollutants such as hydroquinone and catechol [58]. Flexible sensors have significant advantages over rigid analogues in a number of applications and can open up new prospects for on-site analysis and online monitoring. Inspired by that fact and all the considerations above, we developed an electrochemical sensor platform based on LIMPc-plasma-NaOH-Au nanocomposite to detect HQ and CT. Au NPs are recognised for their advantages of easy synthesis, large specific surface area, high chemical stability and good biocompatibility [59,60], which are favorable for the fabrication of sensitive electrochemical sensors [61–64]. Au nanoparticles have a large volume to surface ratio, when placed on the surface of the electrode they can increase their electrochemically active surface area. Moreover, the metallic nature of the nanoparticles can enhance the conductivity of the electrode, improving its sensitivity and selectivity [65,66]. Flexible LIMPc electrodes are synthesized using polyethylene terephthalate (PET), a common food packaging polymer, aluminium nanoparticles (Al NPs) and hydrogen tetrachloroaurate(III). This synthesis process uses widely available and safe materials, providing an environmentally sustainable method that also promotes the recycling of PET. The graphene-based laser-induced metal-polymer composite was treated by Ar/O2 plasma to enhance its wettability and subsequently modified with gold nanoparticles (Au NPs) through electrodeposition. The resulting nanocomposite was characterized using scanning electron microscopy (SEM), X-ray photoelectron spectroscopy (XPS), and various electrochemical techniques, including electrochemical impedance spectroscopy (EIS) and cyclic voltammetry (CV). The sensor's performance was evaluated using differential pulse voltammetry (DPV), which revealed two distinct oxidation peaks. This demonstrated a strong performance for the simultaneous determination of CT and HQ, with good sensitivity, reproducibility, and stability. Furthermore, the sensor was successfully applied to detect CT and HQ in real samples. A schematic diagram illustrating the preparation and detection process is shown in Fig. 1.

2. Materials and methods

2.1. Materials

Hydroquinone ($C_6H_6O_2$, 99 %) was purchased from Macklin Biochemical (Shanghai, China). Catechol ($C_6H_6O_2$, 99 %) was purchased from Thermo Scientific (Massachusetts, USA). Sodium dihydrogen phosphate dihydrate (NaH_2PO_4*$2H_2O$, 98+%), disodium hydrogen phosphate dodecahydrate (Na_2HPO_4*$12H_2O$, 99 %), sodium hydroxide (NaOH, 98 %), hydrogen tetrachloroaurate(III) ($HAuCl_4$, 99.99 %), potassium hexacyanoferrate(II) ($K_4[Fe(CN)_6]$, 98.5 %), potassium chloride (KCl, 99 %) were purchased from Acros Organics (Geel, Belgium). All reagents were analytical grade and used without further purification. Aluminum nanoparticles (AlNPs) were purchased from Advanced Powder Technologies and used as received.

2.2. Synthesis of the LIMPc

LIMPc was synthesized according to a previous report [54]. Briefly, films of AlNPs were drop-casted to a polyethylene terephthalate sheet (0.7 mm thick) from ethanolic dispersion with a concentration of 10 mg/ml (with the amount of 50 μL/cm^2) and dried in ambient conditions. AlNPs act as a photothermal transducer to initiate laser-induced PET pyrolysis for the formation of robust and conductive carbon-based network. AlNPs showed themselves as one of the most promising materials to create LIMPc. The criteria was low electrical resistance along with mechanical and chemical stability. Those films were then subjected to laser-induced carbonization by a 450 nm pulsed laser diode. The thickness of the LIMPc layer fabricated under these conditions is approximately 25 μm [54]. Ater the irradiation, residues of poor integrated into laser-induced carbon network AlNPs were removed by sonication (120 W, 40 kHz) in the distilled water.

A low-pressure plasma treatment technique using Zepto-BRS 200 (Diener electronic) was applied to improve the wettability of the LIMPc. The chamber was filled with Argon (flow rate 10 sccm) containing impurity O_2 (not exceeding 1 %). The plasma treatment time was varied from 1 to 120 sec. The treated sample was assigned as LIMPc-plasma. After plasma treatment, the LIMPc-plasma sample was treated in a 1 M NaOH solution at 60 °C for 30 min. Thus, a LIMPc-plasma-NaOH sample was obtained. Electrodeposition of gold nanoparticles on the samples was carried out using a potentiostatic regime in 1 mM $HAuCl_4$ solution, according to [67]. A constant potential of −0.2 V was applied for 1–60 sec under gentle stirring conditions. After the electrodeposition of gold nanoparticles, the modified electrode was thoroughly rinsed with deionized water. The sample was assigned as LIMPc-plasma-NaOH-Au.

2.3. Characterization techniques

The surface morphology and elemental analysis of the samples were investigated using scanning electron microscopy (SEM) on a Zeiss Merlin (Karl Zeiss) equipped with a field emission cathode, a GEMINI-II electron-optics column, and an INCAx-act energy dispersive X-ray spectrometer (EDX). The qualitative analysis of the samples was characterized using X-ray photoelectron spectroscopy (XPS). The XPS spectra were obtained using ESCALAB 250Xi photoelectron spectrometer with AlKα radiation (photon energy = 1486.6 eV). The Fourier

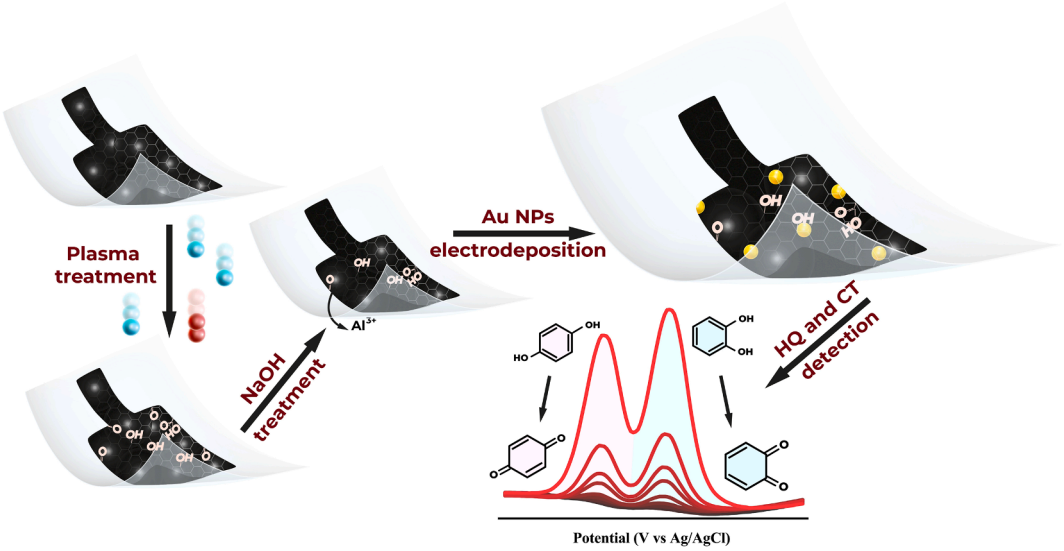

Fig. 1. Schematic presentation of the nanocomposite synthesis and HQ and CT analyses.

transform infrared spectroscopy with attenuated total reflectance (FTIR-ATR) was performed using a Thermo Scientific Nicolet 8700 spectrometer equipped with a diamond crystal. X-ray diffraction (XRD) was carried out using a Bruker D2 Phaser diffractometer.

2.4. Electrochemical measurements

The electrochemical performances of the initial and modified electrodes were studied by cyclic voltammetry (CV), differential pulse voltammetry (DPV) and electrochemical impedance spectroscopy (EIS). Measurements were carried out with Corrtest CS300 potentiostat in a standard three-electrode cell at room temperature (Fig. S1). Platinum foil and Ag/AgCl (3 M KCl) electrodes were used as counter and reference electrodes, respectively. The geometric area of the working electrode was 0.48 cm^2. The contact pad section of the working electrode was coated with epoxy resin to precisely define the working area and to prevent the supporting electrolyte from coming into contact with the contact pad (Fig. S1). The supporting electrolyte was 0.1 M PBS (the preparation protocol of the PBS buffer is included in the Supplementary Information). The CV measurements were recorded at a scan rate of 50 mV/s. The DPV measurements were carried out at amplitude 0.05 V, pulse width 0.05 s, pulse period 0.5 s, inc. E 0.004 V. Analyses were repeated three times (n = 3) where necessary to calculate the relative standard deviation (RSD). The limit of detection (LOD) was calculated using the formula LOD = 3S/b, where S is the standard deviation from linear regression analysis and b is the slope of the calibration curve. The EIS measurements were performed in 5.0 mM $K_4[Fe(CN)_6]$ solution containing 0.1 M KCl across a frequency range from 100 kHz to 0.01 Hz at the open-circuit potential. The amplitude of the applied sinusoidal wave was ± 10 mV. EIS data was fitted using Z-View software. To evaluate EASA, CV curves were obtained at different scan rates from 20 to 120 mV/s in a 0.1 M KCl electrolyte.

2.5. Real sample preparation and analysis

Local tap water samples and pharmaceutical products were used as real samples. Without any pretreatment, tap water samples were diluted with 0.1 M PBS in the ratio of 1:5 [68]. The standard-additions method was registered in tap water with three concentrations of HQ and CT (10, 30 and 100 μM). A skin-lightening cream containing 4 % hydroquinone (Expigment, Türkiye) was used as a pharmaceutical product. 0.1 g of skin-lightening cream was dissolved in 10 ml of H_2O. Then, the solution was filtered through a filter. The filtered solution was analyzed. An aliquot of the obtained solution (0.415, 0.690, 1.380 and 2 ml) was diluted with 0.1 M PBS solution to a volume of 50 ml. The concentration of hydroquinone in each sample was calculated using the linear regression equation of the standard calibration curve.

3. Results

3.1. Characterization of the modified LIMPc

Enhancing the hydrophilicity of the electrode surfaces is crucial for the simultaneous detection of hydroquinone and catechol in water-based electrolytes. Improved sensitivity and repeatability of analysis methods can lead to more reliable measurements. Thus, in this study, plasma treatment with varying durations (0–120 sec) was used to enhance the wettability of the LIMPc. This treatment did not introduce any significant changes to morphology, as evidenced by scanning electron microscopy images (Fig. S2, Fig. 2a–b, d–e). However, a notable decrease in the contact angle was observed after a 30-second treatment (inset photo on Fig. 2). The increased hydrophilicity during plasma treatment is attributed to the formation of oxygen-containing functional groups on the surface [69], as evidenced by X-ray photoelectron spectroscopy (XPS, Fig. 2 c,f). High-resolution C1s region shows rise of sp^3 hybridized carbon components after plasma treatment.

The synthesis protocol of LIMPc requires forming a layer of Al NPs on a polymer surface, which serve as photothermal agents during laser processing, converting laser energy into local heat for PET graphitization. During LIMPc fabrication, Al NPs turn into Al_4C_3-Al_2O_3-Al core–shell structures [54]. Since Al_2O_3 is basically an electrochemically inert material, NaOH treatment was conducted to dissolve Al_2O_3 and Al_4C_3 shells on the electrode's surface revealing blocked active sites. Moreover, exposing the graphene-based material to alkali may lead to carbon corrosion and the formation of defective edges promoting electrochemical activity [70].

EDX mapping showed a decrease in Al content after exposure to NaOH at 60 °C for 30 min (Fig. S3). Increasing the treatment time did not result in further changes, indicating that all accessible aluminum-based components were dissolved.

The morphology of LIMPc, LIMPc-NaOH, and LIMPc-NaOH-Au nanocomposites was characterized using SEM. The images (Fig. 3a, b) demonstrate that LIMPc retains its morphology after exposure to alkali solution. Electrodeposition of gold for three seconds resulted in the formation of uniformly distributed nanoparticles with a size of approximately 20 nm (Fig. 3c–f). The composition of the samples before

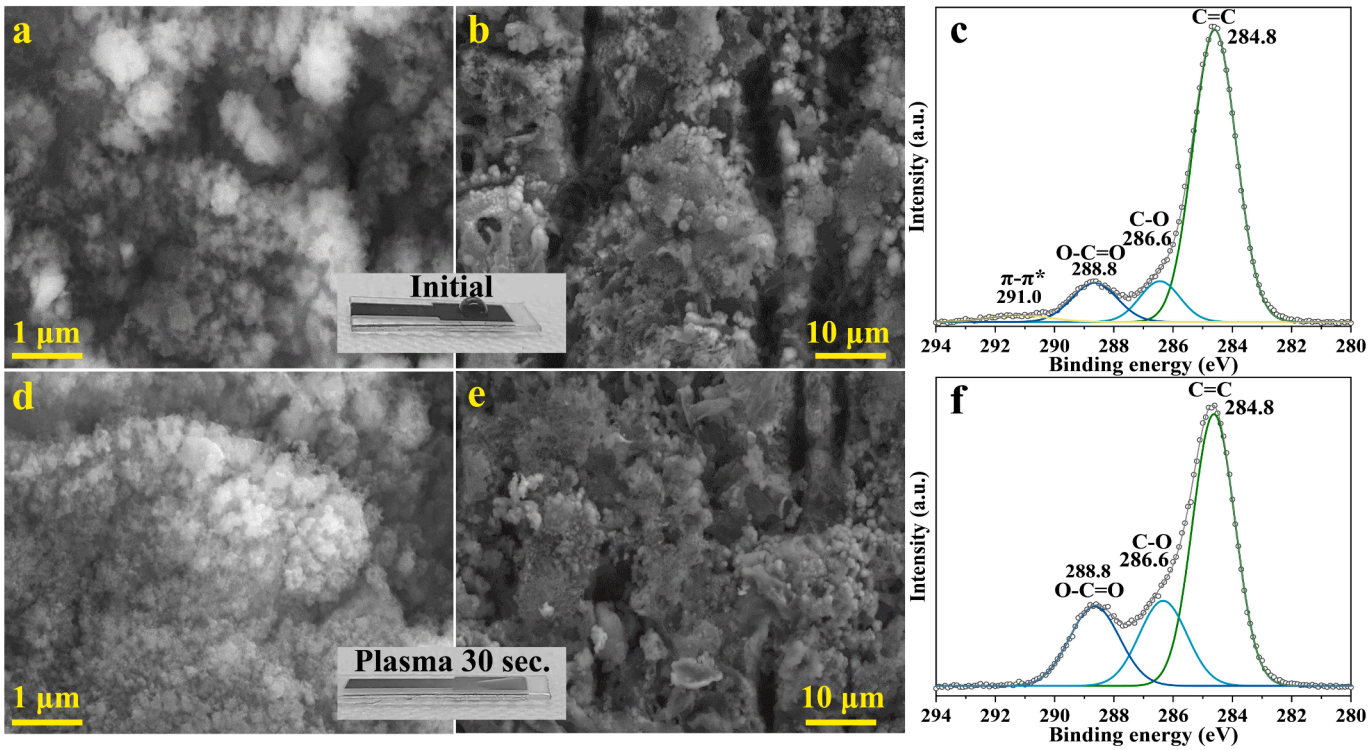

Fig. 2. SEM-images of the electrode surface before (a, b) and after (d, e) 30 s plasma treatment. XPS C1s of LIMPc before (c) and after (f) plasma treatment.

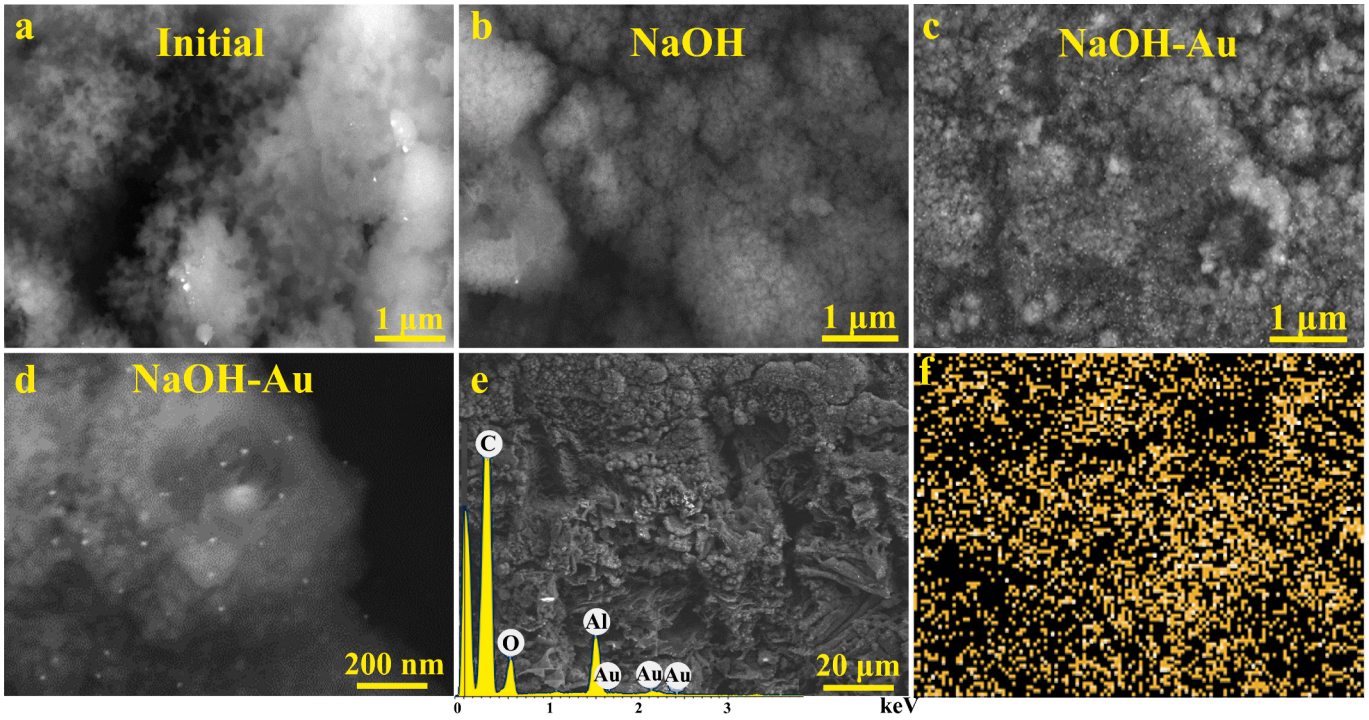

Fig. 3. SEM-images of LIMPc after plasma treatment (a), after NaOH exposure (b), after electrodeposition of gold on the electrode surface for 3 s (c, d). SEM + EDX LIMPc-plasma-NaOH-Au (e), Au distribution on the surface of LIMPc-plasma-NaOH-Au (f).

and after NaOH treatment was characterized by XPS, XRD and FTIR-ATR. The detailed description of XRD and FTIR-ATR results is presented in SI (Fig. S4). The atomic percentage of elemental oxygen (O) was found to be 20.5 for the NaOH-treated samples and 35.4 for the only plasma-treated samples, indicating the partial removal of oxygen during the processing of LIMPc with NaOH (Fig. S5). The π-π* shake-up satellite peak at approximately 291.5 eV reappears after the reaction, which is characteristic of aromatic or conjugated systems. This finding suggests that during the alkali treatment, some of the oxygen-containing functional groups, particularly epoxy and alkoxy groups, were eliminated by NaOH, allowing the restoration of some conjugated bonds [69,70].

3.2. Electrochemical characterization

Cyclic voltammetry (CV) was used to investigate the electron transfer behaviors of LIMPc-plasma, LIMPc-NaOH, and LIMPc-NaOH-Au in a 5.0 mM $[Fe(CN)_6]^{3-/4-}$ redox mediator solution containing 0.1 M KCl (Fig. 4a). For electrochemical testing, only plasma-treated samples were used as they provide reproducible and reliable data. Both LIMPc-plasma-NaOH and LIMPc-plasma-NaOH-Au exhibit superior current responses compared to the LIMPc-plasma. The peak separation (ΔE) values for LIMPc-plasma, LIMPc-plasma-NaOH, and LIMPc-plasma-NaOH-Au are 136 mV, 114 mV, and 70 mV, respectively. The proposed LIMP nanocomposite reduces the overpotentials of CC and HQ and provides excellent peak separation, making it outstanding for the simultaneous detection of both substances. Such performance is attributed to the characteristics of the proposed nanocomposite, which arise from the unique synergistic effect of the developed system. Additionally, the double-layer capacitance (Cdl) increases in the order of LIMPc-plasma, LIMPc-NaOH, and LIMPc-NaOH-Au (Fig. S6), being an evidence of an increase in the electrochemically active surface area (EASA).

Electrochemical impedance spectroscopy (EIS) was used for further analysis of electron transfer behavior (Fig. 4b). The Nyquist plot typically consists of semicircular and linear parts. The semicircle diameter at higher frequencies reflects the resistance value (Rct), indicating the electron transfer process, while the linear section at lower frequencies is associated with the diffusion process. The corresponding equivalent circuit is shown in the inset of Fig. 4b. The electrical element values for all electrodes were obtained by fitting the EIS data using Z-View software (Table S1). The semicircle diameter of LIMPc-plasma is the largest due to its higher resistance, with an Rct value of 45 Ω. In contrast, the Rct values of LIMPc-NaOH and LIMPc-NaOH-Au are lower and equal 25 Ω and 15 Ω, respectively. This reflects that incorporating Au nanoparticles accelerates electron transfer on the electrode surface, thereby increasing electrical conductivity. These findings align with the results obtained from the CV measurements (Fig. S7).

Fig. 4c presents the DPV responses obtained from 0.1 M phosphate-buffered saline (PBS) containing 100 μM hydroquinone (HQ) and 100

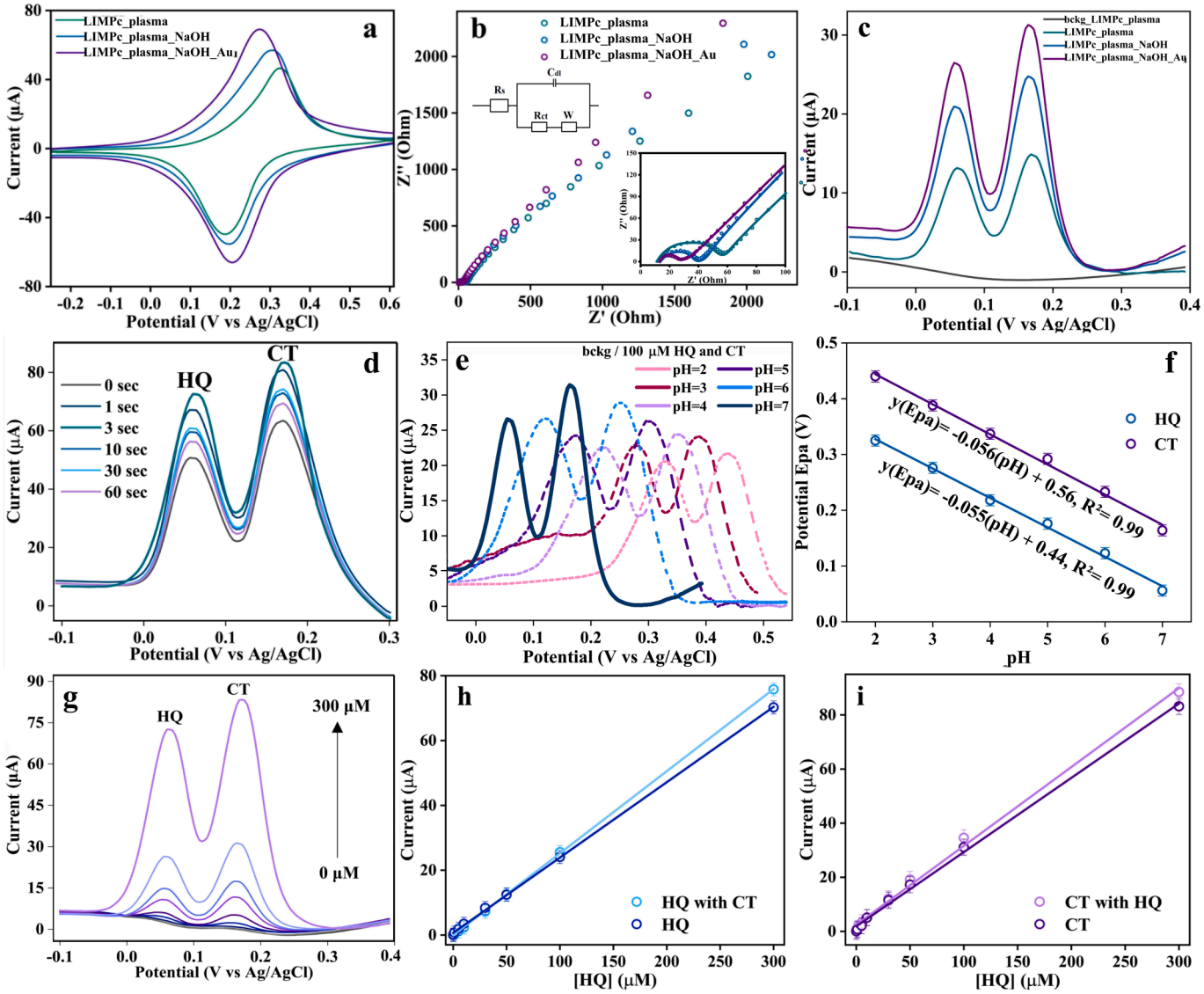

Fig. 4. Electrochemical characterization of LIMPc-plasma, LIMPc-plasma-NaOH, and LIMPc-plasma-NaOH-Au: (a) CVs recorded in 5.0 mM $[Fe(CN)_6]^{3-/4-}$ solution containing 0.1 M KCl; (b) Nyquist plots in 0.1 M KCl with 5.0 mM $K_3[Fe(CN)_6]$ and corresponding equivalent circuit (inset); (c) DPV responses obtained from 0.1 M PBS containing 100 μM HQ and 100 μM CT; (d) DPV of LIMPc-plasma-NaOH-Au electrode recorded in 0.1 M PBS, containing 300 μM HQ and 300 μM CT, at different gold electrodeposition times; (e) DPV of LIMPc-plasma-NaOH-Au electrode containing 100 μM HQ and 100 μM CT at pH = 2–7; (f) Plot of Epa vs. pH containing 100 μM CT and HQ; (g) DPV illustrating the effect of concentrations of CT and HQ (from 0 to 300 μM) in 0.1 M PBS at LIMPc-plasma-NaOH-Au electrode; Dependences of HQ (h) and CT (i) oxidation current on the concentration.

μM catechol (CT) on the LIMPc-plasma, LIMPc-plasma-NaOH, and LIMPc-plasma-NaOH-Au electrodes. Variations in current at lower potentials for studied electrodes, can be attributed to their different compositions. The DPV technique is highly sensitive to the capacitance of the sample; therefore surface modification can affect the DPV response. The LIMPc-plasma electrode exhibits the lowest sensitivity towards HQ and CT detection. In contrast, the LIMPc-plasma-NaOH-Au electrode demonstrates excellent performance by completely separating HQ and CT, with a potential difference of 110 mV. These results indicate that LIMPc-NaOH-Au exhibits the most favorable electrochemical performance among the tested electrodes. Based on the comprehensive characterizations performed, the analytical procedure was further optimized using the LIMPc-plasma-NaOH-Au electrode.

3.3. Optimization of the experiment conditions for CT and HQ detection

Several experimental parameters were examined to improve the performance of the proposed HQ and CT sensor, among them Au NPs loading and pH of the electrolyte solution.

3.3.1. Effect of the Au NPs loading

As the electrodeposition time increases, the loading of gold nanoparticles (Au NPs) on the electrode surface also increases. The current response shows an initial increase of up to 3 s of deposition time, followed by a gradual decline (Fig. 4d). This phenomenon can be attributed to the formation of smaller particles during shorter deposition times compared to longer synthesis procedures (Fig. S8). Smaller NPs have a higher surface-to-volume ratio and a larger number of active sites, resulting in exceptional catalytic and electrocatalytic performances.

3.3.2. pH

The electrooxidation mechanism of CT and HQ has been well studied [71]. These reactions lead to the formation of 1,2-benzoquinone and 1,4-benzoquinone, respectively (Fig. S9). In the case of CT and HQ, the pH of the electrolyte solution plays a significant role, as it affects not only the shape and potential of the peaks but also the peak current [72].

In this study, pH optimization was performed based on the electrocatalytic behavior of the analyte at different pH solutions (from pH = 2 to pH = 7) containing 100 μM HQ and CT (Fig. 4e, Fig. S10). The signal intensity at different pH values is influenced by multiple factors. At lower pH values, the hydroxyl groups of catechol and hydroquinone become protonated (the pKa values are 9.96 for HQ and 9.5 for CT [73]), leading to reduced adsorption on the electrode surface [74]. Additionally, the signal potential of the analytes decreases as the pH increases [75].

Evaluation solutions with pH above 7 was not meaningful due to the low proton availability in alkaline solution and the instability of HQ and CT [76]. Thus, further electrochemical studies were conducted at pH = 7.

The linear regression equation for CT obtained from the calibration curve between anodic peak potential and pH is Epa (CT) = -0.056pH + 0.56 (R^2 = 0.99), for HQ is Epa (HQ) = - 0.055pH + 0.44 (R^2 = 0.99) (Fig. 4f). As observed, the values of the slopes of the calibration straight lines are close to 0.059 (the theoretical value for the Nernst equation). The slopes − 0.055 and − 0.056 are approached to the theoretical value of − 0.059, suggesting that the redox process of HQ and CT has the same electrons and protons involved in the reactions (Fig. S9) [77–79].

3.4. Detection of CT and HQ

The detection of hydroquinone and catechol under optimized conditions was performed using DPV. The choice of DPV for the detection of CC and HQ is based on its advantages of high sensitivity, selectivity, and low background noise, making it ideal for the analysis of these compounds in environmental samples. Fig. 4g displays the DPV response of the LIMPc-plasma-NaOH-Au electrode to HQ and CT with simultaneous variation of HQ and CT concentrations. Additionally, DPVs obtained while maintaining one substance at a constant concentration (30 μM) and altering the concentration of the other substance are presented in the SI (Fig. S11).

The linear regression equation for HQ is given as follows:

Ip (μA) = 0.2739C (μM) + 0.7506, with a regression coefficient of 0.9987. (Fig. 4h)

Similarly, the linear regression equation for CT is:

Ip (μA) = 0.3696C (μM) + 0.2771, with a regression coefficient of 0.9988. (Fig. 4i)

The slope and intercept errors for these equations are presented in Table S2.

The limit of detection for HQ is 0.056 μM, while for CT it is 0.047 μM (S/N = 3). This sensor exhibits superior or comparable characteristics to other reported works, including well-established systems based on modified glassy carbon electrodes [80–88] (Table S3). All the sensors presented in Table S3 have their own advantages, some of them showing a wider linear range or higher sensitivity. This diversity underlines the continuous quest for sensor improvement and highlights the vast potential for further research aimed at finding a system with perfect parameters. The proposed sensor, as detailed in Table S3, exhibits characteristics that are either superior or comparable to those reported in other studies, including low LOD, resistance to interference, exceptional repeatability and long-term stability. In addition, the LIMPc composite has remarkable mechanical flexural strength, which clearly distinguishes our sensor from many similar flexible systems. In addition to excellent analytical performance, the proposed sensor exhibits the advantages of laser-fabricated systems, which consist of precise control over the sensor architecture, providing a cost-effective and versatile alternative to conventional screen-printing and roll-to-roll technologies. The ability to produce sensors of any shape on a variety of surfaces is a significant advantage of laser-based approaches.

3.5. Selectivity, reproducibility, and stability

The influence of interference agents on the determination of 50 μM HQ and 50 μM CT was investigated to evaluate the selectivity of the modified electrode. Table S4 demonstrates that 100-fold concentrations of K^+, Na^+, Fe^{3+}, Zn^{2+}, Mn^{2+}, Al^{3+}, Cr^{3+}, Cu^{2+}, Pb^{2+}, Ni^{2+}, Cl^-, NO_3^-, SO_4^{2-}, PO_4^{3-}, and 1-fold concentrations of phenol, bisphenol A, resorcinol, ascorbic acid, glucose, citric acid and uric acid, diclofenac, nimesulide, acetaminophen (paracetamol), ibuprofen, amoxicillin, levofloxacin, tryptophane, lactic acid, hydrochlorothiazide and valsartan, thiamine and niacinamide, estriol and ethinylestradiol, L-proline and glycine, carbendazim and diquat, pentachlorophenol did not interfere with the simultaneous determination of HQ and CT. The signal changes of HQ and CT were equal to or less than 6.5 % after the addition of interfering substances in the HQ and CT mixture. These results indicate that the LIMPc-plasma-NaOH-Au system exhibits satisfactory anti-interference ability without being influenced by commonly coexisting substances. High selectivity can be achieved by a combination of electrode composition and analytical conditions. The rational design of the composite electrode can significantly increase the selectivity of the sensor. The graphene component enhances the absorption of organic molecules, while the addition of Au NPs facilitates electron transfer, as confirmed by studies with a redox probe. However, it's important not to separate the functions of the composite, as there is a significant contribution from the synergistic effect, which consists in enhancing the properties of the composite components. In addition, selectivity is achieved by careful adjustment of the analytical conditions, including the potential range and the composition of the supporting electrolyte. Stability experiments were conducted over a 30-day period using 50 μM HQ and 50 μM CT (Fig. 5). The DPV peak current exhibited a gradual decrease over time, although all measured peak currents remained above 90 % of the initial ones, suggesting excellent electrode stability (Fig. 5a). In addition, 10 runs using the same sensor in a continuous

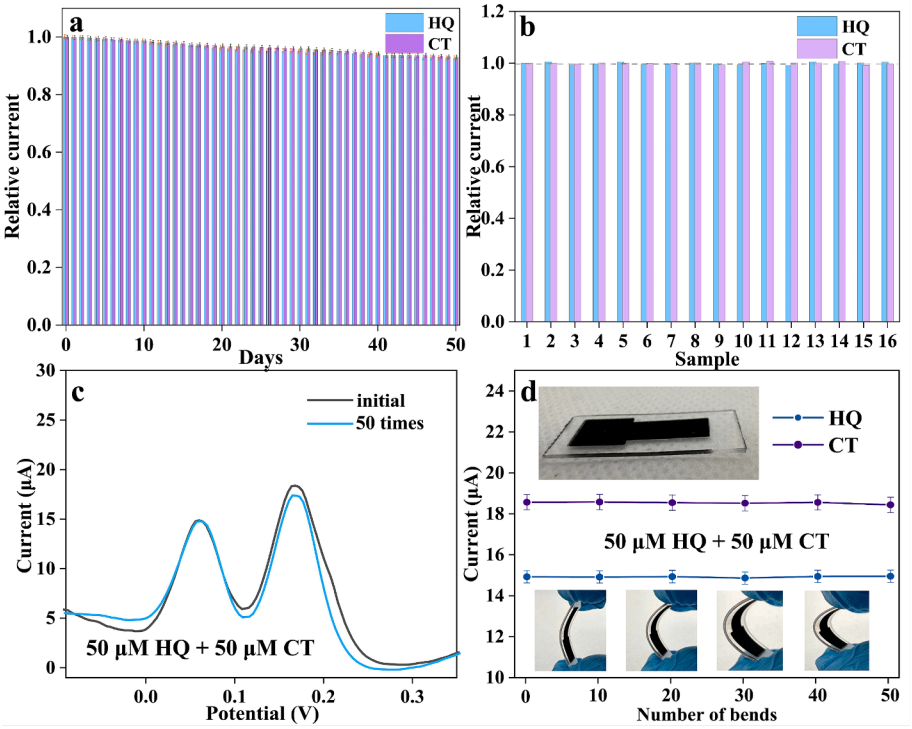

Fig. 5. Investigation of the stability of LIMPc-plasma-NaOH-Au in the presence of 50 μM HQ and CT: Relative value of the peak current DPV of the electrode over 30 days (a); Reproducibility experiment performed with eight different electrodes (b); DPV of the electrode before and after 50 bending cycles (c); Electrochemical response as a function of the number of bending cycles (d).

automated regime were carried out to underline the strong potential of the sensor for real time monitoring applications. The data shown in Fig. S12 indicate that the LIMPc plasma NaOH-Au electrode exhibits exceptional stability over 10 consecutive measurements, with the RSD of the peak current remaining below 2.05 %. Unlike composite electrodes prepared by drop casting nanoparticle suspensions, the proposed LIMPc sensor exhibits high stability due to the inherent integrity of its structure. Laser-induced carbonisation of polyethylene terephthalate provides strong bonding of the fabricated conductive layer to the substrate, resulting in excellent mechanical strength of the material. In addition, electrodeposition also provides strong bonding of Au NPs to the electrode surface and a high degree of stability. Throughout our analyses, we observed that the electrodes remained intact with no evidence of delamination or degradation. Reproducibility experiments were conducted with eight different electrodes for the simultaneous detection of 50 μM HQ and CT (Fig. 5b). The standard deviation of the peak current remained below 3.15 %, supporting the high reproducibility of the proposed sensor. In addition, the influence of temperature variations on the analytical response was also tested (see detailed description in SI). The electrodes showed no noticeable changes in analytical performance when analysis was conducted at elevated temperatures or after exposure of the working electrode to low temperatures (Tables S5–S6).

The flexibility of the LIMPc-plasma-NaOH-Au electrode was investigated by tracking its electrochemical response to catechol and hydroquinone after undergoing up to 50 bending cycles. The flexible LIMPc-plasma-NaOH-Au electrode exhibited minimal impact on the electrochemical responses of CT and HQ, indicating that the sensor possesses excellent flexibility (Fig. 5c, d).

3.6. Spiked and real sample analysis

The practical application of the LIMPc-plasma-NaOH-Au sensor for detecting HQ and CT in real samples was investigated using tap water in the standard addition method. Known concentrations of HQ and CT were added to tap water samples. The calculated recoveries of HQ ranged from 99.7 % to 105.4 %, while the recoveries of CT lie between 98.3 % and 102.0 % (Table S7). The relative standard deviation (RSD) of the tap water detection was found to be less than 2.2 %. These compelling results demonstrate the feasibility and reliability of the sensor for detecting HQ and CT in spiked samples.

Furthermore, to validate the effectiveness of the developed sensor, LIMPc-plasma-NaOH-Au was used for detecting hydroquinone (HQ) in ointment samples intended for treating skin blemishes [89] (Table S8). The manufacturer provided a labeled HQ concentration value of 3.63 mM (40 mg/g). The proposed sensor successfully detected HQ in pharmaceutical ointment with a relative standard deviation (RSD) of 3.5 % (N = 3) and recoveries from 99.5 to 108.1 %, indicating the method's satisfactory accuracy.

4. Conclusion

In this study, we successfully demonstrated a LIMPc-plasma-NaOH-Au-based electrochemical sensor. A comprehensive series of electrochemical tests demonstrated the remarkable electrochemical performance of the flexible electrode, including a wide range and low detection limit for the simultaneous detection of CT and HQ. The sensor exhibits LODs as low as 0.047 μM and 0.056 μM for CT and HQ, respectively. Additionally, the flexible electrode made of LIMPc-plasma-NaOH-Au displayed resistance to interference, excellent repeatability, and long-term stability, making it highly promising for practical CT and HQ detection applications. The potential prospects for further research and improvements of LIMPc electrodes include the fabrication of fully-laser-made sensors for small volume analysis. In addition, targeted modifications, especially with nanomaterials derived from non-precious elements of the LIMP composite, could be considered to broaden its application in electrochemical sensors for a variety of analytes, including biomarkers, pollutants and drugs.

CRediT authorship contribution statement

Maria Kaneva: Writing – review & editing, Validation, Investigation, Formal analysis. **Aleksandra Levshakova:** Writing – review & editing, Visualization. **Ilya Tumkin:** Writing – review & editing. **Maxim Fatkullin:** Writing – review & editing, Investigation. **Evgeny Gurevich:** Writing – review & editing, Methodology. **Alina Manshina:** Writing – review & editing, Supervision. **Raul D. Rodriguez:** Writing – review & editing, Supervision. **Evgeniia Khairullina:** Writing – review & editing, Visualization, Project administration, Methodology, Funding acquisition, Conceptualization.

Declaration of competing interest

The authors declare that they have no known competing financial interests or personal relationships that could have appeared to influence the work reported in this paper.

Data availability

Data will be made available on request.

Acknowledgments

This research was supported by the Russian Science Foundation (grant 23-29-00493).

The authors would also like to thank the SPBU Research Park, especially, Nanotechnology Interdisciplinary Centre, the Centre for Physical Methods of Surface Investigation, and the Centre for Optical and Laser Materials Research.

Appendix A. Supplementary data

Supplementary data to this article can be found online at https://doi.org/10.1016/j.microc.2024.111106.

References

[1] H. Ren, Y. Zhang, L. Liu, Y. Li, D. Wang, R. Zhang, W. Zhang, Y. Li, B.C. Ye, Synthesis of hollow Mo 2 C/carbon spheres, and their application to simultaneous electrochemical detection of hydroquinone, catechol, and resorcinol, Microchim. Acta 186 (2019), https://doi.org/10.1007/s00604-019-3432-7.

[2] S.E. Elugoke, O.E. Fayemi, A.S. Adekunle, B.B. Mamba, T.T.I. Nkambule, E. E. Ebenso, Trends in the analysis, adsorption and transformation of dihydroxybenzenes – A comprehensive review, Microchem. J. 193 (2023), https://doi.org/10.1016/j.microc.2023.108986.

[3] X. Chen, X. Hu, Q. Lu, Y. Yang, S. Linghu, X. Zhang, Study on the differences in sludge toxicity and microbial community structure caused by catechol, resorcinol and hydroquinone with metagenomic analysis, J. Environ. Manage. 302 (2022), https://doi.org/10.1016/j.jenvman.2021.114027.

[4] European Chemicals Agency, Substance Information - Hydroquinone, (2021) 1–5. https://echa.europa.eu/substance-information/-/substanceinfo/100.022.770.

[5] World Health Organization, Hydroquinone Health and Safety Guide, (1996) 101.

[6] D. Periasamy, A. Sundaram, A novel approach for pathogen reduction in wastewater treatment, J. Environ. Heal. Sci. Eng. 11 (2013), https://doi.org/10.1186/2052-336x-11-12.

[7] M.K. Abugazleh, H.M. Ali, J.A. Chester, A.M. Al-Fa'ouri, J.L. Bouldin, Aquatic toxicity of hydroquinone and catechol following metal oxide treatment to Ceriodaphnia dubia and Pimephales promelas, Ecotoxicology 32 (2023), https://doi.org/10.1007/s10646-023-02672-5.

[8] H. Meskher, F. Achi, Electrochemical Sensing Systems for the Analysis of Catechol and Hydroquinone in the Aquatic Environments: A Critical Review, Crit. Rev. Anal. Chem. (2022), https://doi.org/10.1080/10408347.2022.2114784.

[9] M. Wang, R. Guan, S. Jiang, S. Zhang, X. Fan, X. Shao, T. Liu, S. Wang, Q. Yue, Fluorometric assay of hydroquinone without interference from catechol and resorcinol based on carbonized polymer dots, New J. Chem. 47 (2022), https://doi.org/10.1039/d2nj04878g.

[10] S. Fu, Y. Zhu, Y. Zhang, M. Zhang, Y. Zhang, L. Qiao, N. Yin, K. Song, M. Liu, D. Wang, Recent advances in carbon nanomaterials-based electrochemical sensors for phenolic compounds detection, Microchem. J. 171 (2021), https://doi.org/10.1016/j.microc.2021.106776.

[11] D. Manoj, S. Rajendran, T.K.A. Hoang, M. Soto-Moscoso, The role of MOF based nanocomposites in the detection of phenolic compounds for environmental remediation- A review, Chemosphere 300 (2022), https://doi.org/10.1016/j.chemosphere.2022.134516.

[12] L.V.L. Martoni, N.O. Gomes, T.M. Prado, M.L. Calegaro, O.N. Oliveira, S.A. S. Machado, P.A. Raymundo-Pereira, Carbon spherical shells in a flexible photoelectrochemical sensor to determine hydroquinone in tap water, J. Environ. Chem. Eng. 10 (2022), https://doi.org/10.1016/j.jece.2022.107556.

[13] P.A. Raymundo-Pereira, N.O. Gomes, S.A.S. Machado, O.N. Oliveira, Simultaneous, ultrasensitive detection of hydroquinone, paracetamol and estradiol for quality control of tap water with a simple electrochemical method, J. Electroanal. Chem. 848 (2019), https://doi.org/10.1016/j.jelechem.2019.113319.

[14] P.A. Raymundo-Pereira, A.M. Campos, C.D. Mendonça, M.L. Calegaro, S.A. S. Machado, O.N. Oliveira, Printex 6L Carbon Nanoballs used in Electrochemical Sensors for Simultaneous Detection of Emerging Pollutants Hydroquinone and Paracetamol, Sens. Actuators B Chem. 252 (2017), https://doi.org/10.1016/j.snb.2017.05.121.

[15] T. Kokulnathan, A.I. Jothi, S.M. Chen, G. Almutairi, F. Ahmed, N. Arshi, B. AlOtaibi, Integrating graphene oxide with magnesium oxide nanoparticles for electrochemical detection of nitrobenzene, J. Environ. Chem. Eng. 9 (2021), https://doi.org/10.1016/j.jece.2021.106310.

[16] A. Singhal, M.A. Sadique, N. Kumar, S. Yadav, P. Ranjan, A. Parihar, R. Khan, A. K. Kaushik, Multifunctional carbon nanomaterials decorated molecularly imprinted hybrid polymers for efficient electrochemical antibiotics sensing, J. Environ. Chem. Eng. 10 (2022), https://doi.org/10.1016/j.jece.2022.107703.

[17] Y. Luo, M.R. Abidian, J.H. Ahn, D. Akinwande, A.M. Andrews, M. Antonietti, Z. Bao, M. Berggren, C.A. Berkey, C.J. Bettinger, J. Chen, P. Chen, W. Cheng, X. Cheng, S.J. Choi, A. Chortos, C. Dagdeviren, R.H. Dauskardt, C.A. Di, M. D. Dickey, X. Duan, A. Facchetti, Z. Fan, Y. Fang, J. Feng, X. Feng, H. Gao, W. Gao, X. Gong, C.F. Guo, X. Guo, M.C. Hartel, Z. He, J.S. Ho, Y. Hu, Q. Huang, Y. Huang, F. Huo, M.M. Hussain, A. Javey, U. Jeong, C. Jiang, X. Jiang, J. Kang, D. Karnaushenko, A. Khademhosseini, D.H. Kim, I.D. Kim, D. Kireev, L. Kong, C. Lee, N.E. Lee, P.S. Lee, T.W. Lee, F. Li, J. Li, C. Liang, C.T. Lim, Y. Lin, D. J. Lipomi, J. Liu, K. Liu, N. Liu, R. Liu, Y. Liu, Y. Liu, Z. Liu, Z. Liu, X.J. Loh, N. Lu, Z. Lv, S. Magdassi, G.G. Malliaras, N. Matsuhisa, A. Nathan, S. Niu, J. Pan, C. Pang, Q. Pei, H. Peng, D. Qi, H. Ren, J.A. Rogers, A. Rowe, O.G. Schmidt, T. Sekitani, D. G. Seo, G. Shen, X. Sheng, Q. Shi, T. Someya, Y. Song, E. Stavrinidou, M. Su, X. Sun, K. Takei, X.M. Tao, B.C.K. Tee, A.V.Y. Thean, T.Q. Trung, C. Wan, H. Wang, J. Wang, M. Wang, S. Wang, T. Wang, Z.L. Wang, P.S. Weiss, H. Wen, S. Xu, T. Xu, H. Yan, X. Yan, H. Yang, L. Yang, S. Yang, L. Yin, C. Yu, G. Yu, J. Yu, S.H. Yu, X. Yu, E. Zamburg, H. Zhang, X. Zhang, X. Zhang, X. Zhang, Y. Zhang, Y. Zhang, S. Zhao, X. Zhao, Y. Zheng, Y.Q. Zheng, Z. Zheng, T. Zhou, B. Zhu, M. Zhu, R. Zhu, Y. Zhu, Y. Zhu, G. Zou, X. Chen, Technology Roadmap for Flexible Sensors, ACS Nano 17 (2023), https://doi.org/10.1021/acsnano.2c12606.

[18] Q.T. Lai, X.H. Zhao, Q.J. Sun, Z. Tang, X.G. Tang, V.A.L. Roy, Emerging MXene-Based Flexible Tactile Sensors for Health Monitoring and Haptic Perception, Small 19 (2023), https://doi.org/10.1002/smll.202300283.

[19] F. Gao, C. Liu, L. Zhang, T. Liu, Z. Wang, Z. Song, H. Cai, Z. Fang, J. Chen, J. Wang, M. Han, J. Wang, K. Lin, R. Wang, M. Li, Q. Mei, X. Ma, S. Liang, G. Gou, N. Xue, Wearable and flexible electrochemical sensors for sweat analysis: a review, Microsystems Nanoeng. 9 (2023), https://doi.org/10.1038/s41378-022-00443-6.

[20] E.M. Khairullina, K. Ratautas, M.S. Panov, V.S. Andriianov, S. Mickus, A. A. Manshina, G. Račiukaitis, I.I. Tumkin, Laser-assisted surface activation for fabrication of flexible non-enzymatic Cu-based sensors, Microchim. Acta 189 (2022), https://doi.org/10.1007/s00604-022-05347-w.

[21] T. Lin, Y. Xu, A. Zhao, W. He, F. Xiao, Flexible electrochemical sensors integrated with nanomaterials for in situ determination of small molecules in biological samples: A review, Anal. Chim. Acta 1207 (2022), https://doi.org/10.1016/j.aca.2022.339461.

[22] S.C. Teixeira, N.O. Gomes, M.L. Calegaro, S.A.S. Machado, T.V. de Oliveira, N. de Fátima Ferreira, P.-P. Soares, Sustainable plant-wearable sensors for on-site, rapid decentralized detection of pesticides toward precision agriculture and food safety, Biomater. Adv. 155 (2023), https://doi.org/10.1016/j.bioadv.2023.213676.

[23] G. Ibáñez-Redín, G. Rosso Cagnani, N.O. Gomes, P.A. Raymundo-Pereira, S. A. Sergio, M.A. Gutierrez, J.E. Krieger, O.N. Oliveira, Wearable potentiometric biosensor for analysis of urea in sweat, Biosens. Bioelectron. 223 (2023), https://doi.org/10.1016/j.bios.2022.114994.

[24] N.O. Gomes, R.T. Paschoalin, S. Bilatto, A.R. Sorigotti, C.S. Farinas, L.H.C. Mattoso, S.A.S. Machado, O.N. Oliveira, P.A. Raymundo-Pereira, Flexible, Bifunctional Sensing Platform Made with Biodegradable Mats for Detecting Glucose in Urine, ACS Sustain. Chem. Eng. 11 (2023), https://doi.org/10.1021/acssuschemeng.2c05438.

[25] P.A. Raymundo-Pereira, N.O. Gomes, S.A.S. Machado, O.N. Oliveira, Wearable glove-embedded sensors for therapeutic drug monitoring in sweat for personalized medicine, Chem. Eng. J. 435 (2022), https://doi.org/10.1016/j.cej.2022.135047.

[26] R.T. Paschoalin, N.O. Gomes, G.F. Almeida, S. Bilatto, C.S. Farinas, S.A. S. Machado, L.H.C. Mattoso, O.N. Oliveira, P.A. Raymundo-Pereira, Wearable sensors made with solution-blow spinning poly(lactic acid) for non-enzymatic pesticide detection in agriculture and food safety, Biosens. Bioelectron. 199 (2022), https://doi.org/10.1016/j.bios.2021.113875.

[27] P.A. Raymundo-Pereira, N.O. Gomes, M. Shimizu, A. Sergio, Selective and sensitive multiplexed detection of pesticides in food samples using wearable, flexible glove-embedded non-enzymatic sensors, Chem. Eng. J. 408 (2021) 127279, https://doi.org/10.1016/j.cej.2020.127279.

[28] R.R. Silva, P.A. Raymundo-Pereira, A.M. Campos, D. Wilson, C.G. Otoni, H. S. Barud, C.A.R. Costa, R.R. Domeneguetti, D.T. Balogh, S.J.L. Ribeiro, O. N. Oliveira, Microbial nanocellulose adherent to human skin used in

electrochemical sensors to detect metal ions and biomarkers in sweat, Talanta 218 (2020), https://doi.org/10.1016/j.talanta.2020.121153.
[29] N.O. Gomes, S.C. Teixeira, M.L. Calegaro, S.A.S. Machado, N. de Fátima Ferreira, T. V. de Soares, P.-P. Oliveira, Flexible and sustainable printed sensor strips for on-site, fast decentralized self-testing of urinary biomarkers integrated with a portable wireless analyzer, Chem. Eng. J. 472 (2023), https://doi.org/10.1016/j.cej.2023.144775.
[30] A.M. de Campos, R.R. Silva, M.L. Calegaro, P.A. Raymundo-Pereira, Design and Fabrication of Flexible Copper Sensor Decorated with Bismuth Micro/Nanodentrites to Detect Lead and Cadmium in Noninvasive Samples of Sweat, Chemosensors 10 (2022), https://doi.org/10.3390/chemosensors10110446.
[31] N.O. Gomes, P.A. Raymundo-Pereira, On-Site Therapeutic Drug Monitoring of Paracetamol Analgesic in Non-Invasively Collected Saliva for Personalized Medicine, Small 19 (2023), https://doi.org/10.1002/smll.202206753.
[32] P.A. Raymundo-Pereira, N.O. Gomes, J.H.S. Carvalho, S.A.S. Machado, O. N. Oliveira, B.C. Janegitz, Simultaneous Detection of Quercetin and Carbendazim in Wine Samples Using Disposable Electrochemical Sensors, ChemElectroChem 7 (2020), https://doi.org/10.1002/celc.202000788.
[33] L.V.L. Martoni, N.O. Gomes, O.N. Oliveira, S.A.S. Machado, P.A. Raymundo-Pereira, Low-cost photoelectrochemical sensor sensitized with carbon spherical shells and cobalt(II) phthalocyanine for fast acetaminophen determination, Microchem. J. 197 (2024), https://doi.org/10.1016/j.microc.2023.109780.
[34] N.O. Gomes, C.D. Mendonça, S.A.S. Machado, O.N. Oliveira, P.A. Raymundo-Pereira, Flexible and integrated dual carbon sensor for multiplexed detection of nonylphenol and paroxetine in tap water samples, Microchim. Acta 188 (2021), https://doi.org/10.1007/s00604-021-05024-4.
[35] S.C. Teixeira, N.O. Gomes, T.V. de Oliveira, P. Fortes-Da-Silva, N. de F.F. Soares, P. A. Raymundo-Pereira, Review and Perspectives of sustainable, biodegradable, eco-friendly and flexible electronic devices and (Bio)sensors, Biosens. Bioelectron. X 14 (2023), https://doi.org/10.1016/j.biosx.2023.100371.
[36] O. Guselnikova, O. Semyonov, E. Sviridova, R. Gulyaev, A. Gorbunova, D. Kogolev, A. Trelin, Y. Yamauchi, R. Boukherroub, P. Postnikov, "Functional upcycling" of polymer waste towards the design of new materials, Chem. Soc. Rev. 52 (2023), https://doi.org/10.1039/d2cs00689h.
[37] C. Jehanno, J.W. Alty, M. Roosen, S. De Meester, A.P. Dove, E.Y.X. Chen, F. A. Leibfarth, H. Sardon, Critical advances and future opportunities in upcycling commodity polymers, Nature 603 (2022), https://doi.org/10.1038/s41586-021-04350-0.
[38] Q. Hou, M. Zhen, H. Qian, Y. Nie, X. Bai, T. Xia, M. Laiq Ur Rehman, Q. Li, M. Ju, Upcycling and catalytic degradation of plastic wastes, Cell Reports Phys. Sci. 2 (2021), https://doi.org/10.1016/j.xcrp.2021.100514.
[39] A.K. Singh, R. Bedi, B.S. Kaith, Composite materials based on recycled polyethylene terephthalate and their properties – A comprehensive review, Compos. Part B Eng. 219 (2021), https://doi.org/10.1016/j.compositesb.2021.108928.
[40] A. Garg, P. Somani, A. Gaur, B.L. Swami, Gainful utilization of plastic waste in dense bituminous macadam, IOP Conf. Ser. Mater. Sci. Eng. (2020), https://doi.org/10.1088/1757-899X/872/1/012129.
[41] O. Vieira, R.S. Ribeiro, J.L. Diaz de Tuesta, H.T. Gomes, A.M.T. Silva, A systematic literature review on the conversion of plastic wastes into valuable 2D graphene-based materials, Chem. Eng. J. 428 (2022), https://doi.org/10.1016/j.cej.2021.131399.
[42] C. Wang, H. Han, Y. Wu, D. Astruc, Nanocatalyzed upcycling of the plastic wastes for a circular economy, Coord. Chem. Rev. 458 (2022), https://doi.org/10.1016/j.ccr.2022.214422.
[43] S. Ren, X. Xu, K. Hu, W. Tian, X. Duan, J. Yi, S. Wang, Structure-oriented conversions of plastics to carbon nanomaterials, Carbon Res. 1 (2022), https://doi.org/10.1007/s44246-022-00016-2.
[44] A.C. Bressi, A. Dallinger, Y. Steksova, F. Greco, Bioderived Laser-Induced Graphene for Sensors and Supercapacitors, ACS Appl. Mater. Interfaces 15 (2023), https://doi.org/10.1021/acsami.3c07687.
[45] E. Koukouviti, D. Soulis, A. Economou, C. Kokkinos, Wooden Tongue Depressor Multiplex Saliva Biosensor Fabricated via Diode Laser Engraving, Anal. Chem. 95 (2023), https://doi.org/10.1021/acs.analchem.3c01211.
[46] D. Kogolev, O. Semyonov, N. Metalnikova, M. Fatkullin, R.D. Rodriguez, P. Slepicka, Y. Yamauchi, O. Guselnikova, R. Boukherroub, P.S. Postnikov, Waste PET upcycling to conductive carbon-based composite through laser-assisted carbonization of UiO-66, J. Mater. Chem. A 11 (2022), https://doi.org/10.1039/d2ta08127j.
[47] E.A. Avilova, E.M. Khairullina, A.Y. Shishov, E.A. Eltysheva, V. Mikhailovskii, D. A. Sinev, I.I. Tumkin, Direct Laser Writing of Copper Micropatterns from Deep Eutectic Solvents Using Pulsed near-IR Radiation, Nanomaterials 12 (2022) 1–12, https://doi.org/10.3390/nano12071127.
[48] M. Mizoshiri, K. Yoshidomi, N. Darkhanbaatar, E.M. Khairullina, I.I. Tumkin, Effect of substrates on femtosecond laser pulse-induced reductive sintering of cobalt oxide nanoparticles, Nanomaterials 11 (2021), https://doi.org/10.3390/nano11123356.
[49] A.S. Levshakova, E.M. Khairullina, L.S. Logunov, M.S. Panov, A.S. Mereshchenko, V.B. Sosnovsky, D.I. Gordeychuk, A.Y. Shishov, I.I. Tumkin, Highly rapid direct laser fabrication of Ni micropatterns for enzyme-free sensing applications using deep eutectic solvent, Mater. Lett. 308 (2022), https://doi.org/10.1016/j.matlet.2021.131085.
[50] Y. Borodaenko, S. Syubaev, E. Khairullina, I. Tumkin, S. Gurbatov, A. Mironenko, E. Mitsai, A. Zhizhchenko, E. Modin, E.L. Gurevich, A.A. Kuchmizhak, On-Demand Plasmon Nanoparticle-Embedded Laser-Induced Periodic Surface Structures (LIPSSs) on Silicon for Optical Nanosensing, Adv. Opt. Mater. 10 (2022), https://doi.org/10.1002/adom.202201094.
[51] X. Zhou, W. Guo, Y. Yao, R. Peng, P. Peng, Flexible Nonenzymatic Glucose Sensing with One-Step Laser-Fabricated Cu2O/Cu Porous Structure, Adv. Eng. Mater. 23 (2021), https://doi.org/10.1002/adem.202100192.
[52] B. Yoo, D. Bowen, N. Lazarus, D. Pines, Laser Direct Structured 3D Circuits on Silicone, ACS Appl. Mater. Interfaces 14 (2022), https://doi.org/10.1021/acsami.2c01029.
[53] J. Liao, W. Guo, P. Peng, Direct laser writing of copper-graphene composites for flexible electronics, Opt. Lasers Eng. 142 (2021), https://doi.org/10.1016/j.optlaseng.2021.106605.
[54] R.D. Rodriguez, S. Shchadenko, G. Murastov, A. Lipovka, M. Fatkullin, I. Petrov, T. H. Tran, A. Khalelov, M. Saqib, N.E. Villa, V. Bogoslovskiy, Y. Wang, C.G. Hu, A. Zinovyev, W. Sheng, J.J. Chen, I. Amin, E. Sheremet, Ultra-Robust Flexible Electronics by Laser-Driven Polymer-Nanomaterials Integration, Adv. Funct. Mater. 31 (2021), https://doi.org/10.1002/adfm.202008818.
[55] M. Fatkullin, R.D. Rodriguez, I. Petrov, N.E. Villa, A. Lipovka, M. Gridina, G. Murastov, A. Chernova, E. Plotnikov, A. Averkiev, D. Cheshev, O. Semyonov, F. Gubarev, K. Brazovskiy, W. Sheng, I. Amin, J. Liu, X. Jia, E. Sheremet, Molecular Plasmonic Silver Forests for the Photocatalytic-Driven Sensing Platforms, Nanomaterials 13 (2023), https://doi.org/10.3390/nano13050923.
[56] W. Yang, H. Guo, T. Fan, X. Zhao, L. Zhang, Q. Guan, N. Wu, Y. Cao, W. Yang, MoS2/Ni(OH)2 composites derived from in situ grown Ni-MOF coating MoS2 as electrode materials for supercapacitor and electrochemical sensor, Colloids Surfaces A Physicochem. Eng. Asp. 615 (2021), https://doi.org/10.1016/j.colsurfa.2021.126178.
[57] G. Liu, J. Liu, P. Pan, Z. Wang, Z. Yang, J. Wei, P. Li, S. Cao, H. Shen, J. Zhou, X. Zhang, Electrochemical sensor based on laser-induced preparation of MnOx/rGO composites for simultaneous recognition of hydroquinone and catechol, Microchem. J. 185 (2023), https://doi.org/10.1016/j.microc.2022.108234.
[58] A.C. de Sá, S.C. Barbosa, P.A. Raymundo-Pereira, D. Wilson, F.M. Shimizu, M. Raposo, O.N. Oliveira, Flexible carbon electrodes for electrochemical detection of bisphenol-a, hydroquinone and catechol in water samples, Chemosensors 8 (2020), https://doi.org/10.3390/chemosensors8040103.
[59] H. Yuan, W. Ji, S. Chu, S. Qian, F. Wang, J.F. Masson, X. Han, W. Peng, Fiber-optic surface plasmon resonance glucose sensor enhanced with phenylboronic acid modified Au nanoparticles, Biosens. Bioelectron. 117 (2018), https://doi.org/10.1016/j.bios.2018.06.042.
[60] A.P. Paradis, A. Petruk, G. Sciaini, E. Krivoshapkina, A. Lee, A. Klinkova, An aligned octahedral core in a nanocage: synthesis, plasmonic, and catalytic properties, Nanoscale 11 (2019) 3138–3144, https://doi.org/10.1039/c8nr09731c.
[61] S. Palanisamy, K. Thangavelu, S.M. Chen, B. Thirumalraj, X.H. Liu, Preparation and characterization of gold nanoparticles decorated on graphene oxide@polydopamine composite: Application for sensitive and low potential detection of catechol, Sensors Actuat. B Chem. 233 (2016), https://doi.org/10.1016/j.snb.2016.04.083.
[62] T. Xiao, J. Huang, D. Wang, T. Meng, X. Yang, Au and Au-Based nanomaterials: Synthesis and recent progress in electrochemical sensor applications, Talanta 206 (2020), https://doi.org/10.1016/j.talanta.2019.120210.
[63] M.S. Panov, E.M. Khairullina, F.S. Vshivtcev, M.N. Ryazantsev, I.I. Tumkin, Laser-induced synthesis of composite materials based on iridium, gold and platinum for non-enzymatic glucose sensing, Materials (Basel) 13 (2020), https://doi.org/10.3390/ma13153359.
[64] E.M. Khairullina, I.I. Tumkin, D.D. Stupin, A.V. Smikhovskaia, A.S. Mereshchenko, A.I. Lihachev, A.V. Vasin, M.N. Ryazantsev, M.S. Panov, Laser-Assisted Surface Modification of Ni Microstructures with Au and Pt toward Cell Biocompatibility and High Enzyme-Free Glucose Sensing, ACS Omega 6 (2021), https://doi.org/10.1021/acsomega.1c01880.
[65] Y. Tang, R. Huang, C. Liu, S. Yang, Z. Lu, S. Luo, Electrochemical detection of 4-nitrophenol based on a glassy carbon electrode modified with a reduced graphene oxide/Au nanoparticle composite, Anal. Methods 5 (2013), https://doi.org/10.1039/c3ay40742j.
[66] T.C. Canevari, P.A. Raymundo-Pereira, R. Landers, S.A.S. Machado, Direct synthesis of Ag nanoparticles incorporated on a mesoporous hybrid material as a sensitive sensor for the simultaneous determination of dihydroxybenzenes isomers, Eur. J. Inorg. Chem. (2013), https://doi.org/10.1002/ejic.201300879.
[67] S. Erogul, S.Z. Bas, M. Ozmen, S. Yildiz, A new electrochemical sensor based on Fe3O4 functionalized graphene oxide-gold nanoparticle composite film for simultaneous determination of catechol and hydroquinone, Electrochim. Acta 186 (2015), https://doi.org/10.1016/j.electacta.2015.10.174.
[68] N.S. Prinith, J.G. Manjunatha, A.A. Al-Kahtani, A.M. Tighezza, M. Sillanpää, Highly Selective and Sensitive Voltammetric Method for the Detection of Catechol in Tea and Water Samples Using Poly(gibberellic acid)-Modified Carbon Paste Electrode, ACS Omega 7 (2022), https://doi.org/10.1021/acsomega.2c02553.
[69] S.A. Evlashin, J.V. Bondareva, T.F. Aslyamov, Y.V. Lyulin, K.I. Maslakov, K. V. Mironovich, M.A. Tarkhov, H. Ouerdane, Plasma modification of carbon nanowalls induces transition from superhydrophobic to superhydrophilic, Nanotechnology 32 (2021), https://doi.org/10.1088/1361-6528/ac153f.
[70] L. Huang, Y. Cao, D. Diao, Electrochemical activation of graphene sheets embedded carbon films for high sensitivity simultaneous determination of hydroquinone, catechol and resorcinol, Sens. Actuat. B Chem. 305 (2020), https://doi.org/10.1016/j.snb.2019.127495.
[71] A.R. Lopes Da Silva, A. Jhones Dos Santos, C.A. Martínez-Huitle, Electrochemical measurements and theoretical studies for understanding the behavior of catechol,

resorcinol and hydroquinone on the boron doped diamond surface, RSC Adv. 8 (2018), https://doi.org/10.1039/c7ra12257h.
[72] S.A.B. Bukhari, H. Nasir, L. Pan, M. Tasawar, M. Sohail, M. Shahbaz, F. Gul, E. Sitara, Supramolecular assemblies of carbon nanocoils and tetraphenylporphyrin derivatives for sensing of catechol and hydroquinone in aqueous solution, Sci. Rep. 11 (2021), https://doi.org/10.1038/s41598-021-84294-7.
[73] Q. Li, H. An, Q. Zhang, H. Cui, D. Tao, Z. Wei, J. Zhai, Performance of Chloride Ions on Electrocatalytic Oxidation Process Using Ti-Nanotubes/PDDA-PbO2 Anode for Phenol Removal, J. Environ. Eng. 139 (2013), https://doi.org/10.1061/(asce)ee.1943-7870.0000740.
[74] M. Zhang, C.Y. Ge, Y.F. Jin, L. Bin Hu, H.Z. Mo, X.B. Li, H. Zhang, Sensitive and Simultaneous Determination of Hydroquinone and Catechol in Water Using an Anodized Glassy Carbon Electrode with Polymerized 2-(Phenylazo), Chromotropic Acid, J. Chem. 2019 (2019), https://doi.org/10.1155/2019/2327064.
[75] G. Wang, S. Zhang, Q. Wu, J. Zhu, S. Chen, Y. Lei, Y. Li, H. Yi, L. Chen, Z.Q. Shi, Y. Xiao, Simultaneous detection of acetaminophen, catechol and hydroquinone using a graphene-assisted electrochemical sensor, RSC Adv. 12 (2022), https://doi.org/10.1039/d2ra03900a.
[76] J. Fan, J. Pang, Y. Zhang, L. Zhang, W. Xu, J. Wang, Simultaneous detection of hydroquinone and catechol with decreasing pH at a bare glassy carbon electrode surface, Anal. Methods 11 (2019), https://doi.org/10.1039/c8ay02419g.
[77] H. Mao, M. Liu, Z. Cao, C. Ji, Y. Sun, D. Liu, S. Wu, Y. Zhang, X.M. Song, Poly(4-vinylphenylboronic acid) functionalized polypyrrole/graphene oxide nanosheets for simultaneous electrochemical determination of catechol and hydroquinone, Appl. Surf. Sci. 420 (2017), https://doi.org/10.1016/j.apsusc.2017.05.188.
[78] B. Nasr, G. Abdellatif, P. Cañizares, C. Sáez, J. Lobato, M.A. Rodrigo, Electrochemical oxidation of hydroquinone, resorcinol, and catechol on boron-doped diamond anodes, Environ. Sci. Technol. 39 (2005), https://doi.org/10.1021/es0500660.
[79] Y. Feng, C. Sen Zhao, S.H. Cao, S.H. Cai, H.J. Sun, Z. Chen, The electrochemical oxidation of hydroquinone and catechol through polyaniline and poly(aspartic acid) thin films: A comparative study, AIP Adv. 8 (2018), https://doi.org/10.1063/1.5042135.
[80] S. Nagarajan, R. Vairamuthu, R. Angamuthu, G. Venkatachalam, Electrochemical fabrication of reusable pencil graphite electrodes for highly sensitive, selective and simultaneous determination of hydroquinone and catechol, J. Electroanal. Chem. 846 (2019), https://doi.org/10.1016/j.jelechem.2019.05.038.
[81] D. Cheng, X. Kan, Simultaneous determination of dihydroxybenzene isomers based on gold dendritic/pEDOT electrochemical sensor, J. Electroanal. Chem. 857 (2020), https://doi.org/10.1016/j.jelechem.2019.113741.
[82] C.M. Kuskur, B.E. Kumara Swamy, H. Jayadevappa, Poly (Evans blue) sensor for catechol and hydroquinone: A voltammetric study, J. Electroanal. Chem. 833 (2019), https://doi.org/10.1016/j.jelechem.2018.12.012.
[83] Z. Wang, M. Li, Y. Ye, Y. Yang, Y. Lu, X. Ma, Z. Zhang, S. Xiang, MOF-derived binary mixed carbon/metal oxide porous materials for constructing simultaneous determination of hydroquinone and catechol sensor, J. Solid State Electrochem. 23 (2019) 81–89, https://doi.org/10.1007/s10008-018-4111-z.
[84] J. Zuo, Y. Shen, L. Wang, Q. Yang, Z. Cao, H. Song, Z. Ye, S. Zhang, Flexible electrochemical sensor constructed using an active copper center instead of unstable molybdenum carbide for simultaneous detection of toxic catechol and hydroquinone, Microchem. J. 187 (2023), https://doi.org/10.1016/j.microc.2023.108443.
[85] L. Fan, X. Li, X. Kan, Disposable graphite paper based sensor for sensitive simultaneous determination of hydroquinone and catechol, Electrochim. Acta 213 (2016), https://doi.org/10.1016/j.electacta.2016.06.096.
[86] C.C. Maciel, L.F. de Lima, A.L. Ferreira, W.R. de Araujo, M. Ferreira, Development of a flexible and disposable electrochemical sensor based on poly (butylene adipate-co-terephthalate) and graphite for hydroquinone sensing, Sens. Actuat. Rep. 4 (2022), https://doi.org/10.1016/j.snr.2022.100091.
[87] M. Buleandra, A.A. Rabinca, C. Mihailciuc, A. Balan, C. Nichita, I. Stamatin, A. A. Ciucu, Screen-printed Prussian Blue modified electrode for simultaneous detection of hydroquinone and catechol, Sensors Actuators, B Chem. 203 (2014), https://doi.org/10.1016/j.snb.2014.07.043.
[88] I.A. de Araujo Andreotti, L.O. Orzari, J.R. Camargo, R.C. Faria, L.H. Marcolino-Junior, M.F. Bergamini, A. Gatti, B.C. Janegitz, Disposable and flexible electrochemical sensor made by recyclable material and low cost conductive ink, J. Electroanal. Chem. 840 (2019), https://doi.org/10.1016/j.jelechem.2019.03.059.
[89] V. Movahed, L. Arshadi, M. Rezaei, Simultaneous electrochemical detection of antioxidants Hydroquinone, Mono-Tert-butyl hydroquinone and catechol in food and polymer samples using ZnO@MnO2-rGO nanocomposite as sensing layer, Food Chem. (2023), https://doi.org/10.1016/j.foodchem.2022.134286.